Audio Engineering Society

Convention Paper 7989

Presented at the 128th Convention
2010 May 22–25 London, UK

Modeling a loudspeaker as a flexible spherical cap on a rigid sphere

Ronald M. Aarts[1,2], and Augustus J.E.M. Janssen[2,3]

[1] *Philips Research Europe, HTC 36 (WO-02), NL-5656AE Eindhoven, The Netherlands*

[2] *Technical University Eindhoven, Dept. EE, Den Dolech 2, PT, P.O Box 513, NL-5600 MB Eindhoven, The Netherlands*

[3] *Technical University Eindhoven, Dept. EURANDOM, Den Dolech 2, LG-1, P.O Box 513, NL-5600 MB Eindhoven, The Netherlands*

Correspondence should be addressed to Ronald M. Aarts (`Ronald.M.Aarts@philips.com`)

ABSTRACT

It has been argued that the sound radiation of a loudspeaker is modeled realistically by assuming the loudspeaker cabinet to be a rigid sphere with a moving rigid spherical cap. Series expansions, valid in the whole space on and outside the sphere, for the pressure due to a harmonically excited, flexible cap with an axially symmetric velocity distribution are presented. The velocity profile is expanded in functions orthogonal on the cap rather than on the whole sphere. This has the advantage that only a few expansion coefficients are sufficient to accurately describe the velocity profile. An adaptation of the standard solution of the Helmholtz equation to this particular parametrization is required. This is achieved by using recent results on argument scaling in orthogonal Zernike polynomials. The efficacy of the approach is exemplified by calculating various acoustical quantities with particular attention to certain velocity profiles that vanish at the rim of the cap to a desired degree. These quantities are: the sound pressure, polar response, baffle-step response, sound power, directivity, and acoustic center of the radiator. The associated inverse problem, in which the velocity profile is estimated from pressure measurements around the sphere, is feasible as well since the number of expansion coefficients to be estimated is limited. This is demonstrated with a simulation.

1. INTRODUCTION

The sound radiation of a loudspeaker is commonly modeled by assuming the loudspeaker cabinet to be a rigid infinite baffle around a circularly symmetric membrane. Given a velocity distribution on the membrane, the pressure in front of the baffle due to a harmonic excitation is then described by the Rayleigh integral [1] or by King's integral [2]. These integrals have given rise to an impressive arsenal of analytic results and numerical methods to determine the pressure and other acoustical quantities in journal papers [3, 4, 5, 6, 7, 8, 9, 10, 11, 13, 14, 15, 16, 17, 12, 18, 19, 20, 21] and textbooks [22, 23, 24, 25, 26, 27, 28]. The results thus obtained are in good correspondence with what one finds, numerically or otherwise, when the loudspeaker is modeled as being a finite-extent box-like cabinet with a circular, vibrating membrane. Here one should, however, limit attention to the region in front of the loudspeaker and not too far from the axis through the middle of and perpendicular to the membrane. The validity of the infinite-baffle model becomes questionable, or even nonsensical, on the side region or behind the loudspeaker [26, p. 181]. An alternative model, with potential for more adequately dealing with the latter regions, assumes the loudspeaker to be a rigid sphere equipped with a membrane in a spherical cap of the sphere.

It has been argued by Morse and Ingard [24, Sec. 7.2], that using the sphere as a simplified model of a loudspeaker whose cabinet has roughly the same width, height and depth, produces comparable acoustical results as the true loudspeaker. This is illustrated in Fig. 1, where the polar plots are shown for (a) a real measured driver in a rectangular cabinet, (b) a rigid piston in an infinite baffle, and (c) a rigid spherical cap in a rigid sphere. In Sec. 2 this will be discussed in more detail, but it can already be said that the plots clearly show that the agreement between the polar plots of the loudspeaker (a) and the spherical cap (c) is much larger than between the plots of the loudspeaker (a) and the piston (b). An application for the cap model is that it can be used to predict the polar behavior of a loudspeaker cabinet.

Modeling the loudspeaker as a flexible spherical cap on a rigid sphere has the attractive feature that the solution of the Helmholtz equation for the pressure

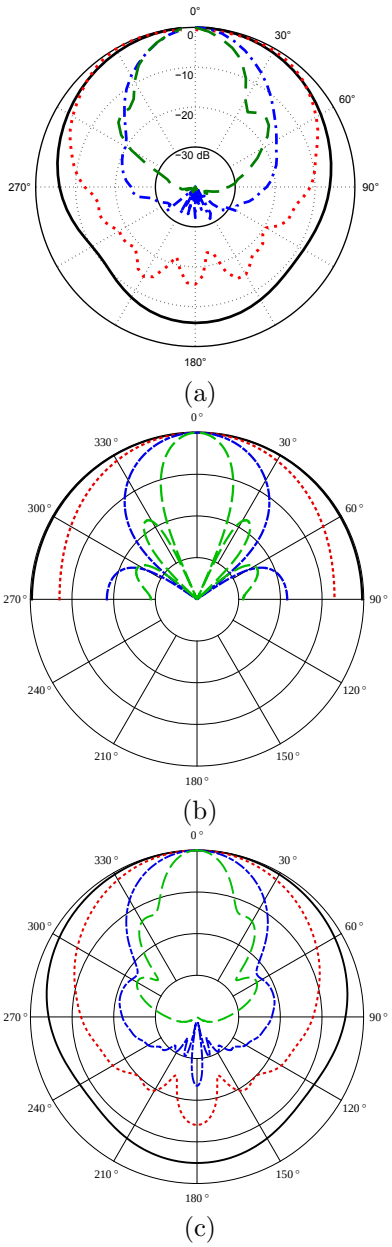

Fig. 1: Polar plots of the SPL (10 dB/div.), f= 1 kHz (solid curve), 4 kHz (dotted curve), 8 kHz (dashed-dotted curve), and 16 kHz (dashed curve), corresponding for c = 340 m/s and a = 3.2 cm to ka values: 0.591, 2.365, 4.731, 9.462. All curves are normalized such that the SPL is 0 dB at θ=0. (a) Loudspeaker radius a = 3.2 cm, measuring distance r = 1 m) in rectangular cabinet, (b) Rigid piston (a = 3.2 cm) in infinite baffle, (c) Rigid spherical cap (aperture $\theta_0 = \pi/8$, sphere radius R = 8.2 cm, r = 1 m, corresponding to kR values: 1.5154, 6.0614, 12.1229, 24.2457) using Eqs. (7) and (11). The parameters a, R, and θ_0 are such—using Eq. (13)—that the area of the piston and the cap are equal.

is feasible in terms of spherical harmonics and spherical Hankel functions, see Ref. [22, Ch.11.3], Ref. [23, Ch. III, Sec. 6], Ref. [24, Ch. 7] and Ref. [25, Chs. 19–20]. In Ref. [7] there is a discussion on how the polar cap model for sphere radius $R \to \infty$ agrees with the model that starts from the flat piston in an infinite baffle. When the cap aperture θ approaches π, the solution becomes that of the simple pulsating sphere. Hence, the polar-cap solution subsumes the solutions of the two classic radiation problems. The mathematical results in Ref. [7] comprise the product kR in a crucial way. The authors of Ref. [7] emphasize that, physically, the case that $kR \to \infty$ with wave number k fixed and $R \to \infty$ differs from the case that $kR \to \infty$ with both $k \to \infty,\ R \to \infty$. This very same issue, for the case of a piston, has been addressed by Rogers and Williams [4].

In the present paper, the velocity profile is assumed to be axially symmetric but otherwise general. It was shown by Frankort [29] that this is a realistic assumption for loudspeakers, because their cones mainly vibrate in a radially symmetric fashion. These loudspeaker velocity profiles can be parameterized conveniently and efficiently in terms of expansion coefficients relative to functions orthogonal on the cap. Using the standard solution of the Helmholtz equation with spherical boundary conditions, a formula will be developed, explicitly involving these expansion coefficients, for the pressure at any point on and outside the sphere.

In the next section (Sec. 2) a detailed overview of the geometry and the basic formulas is given. In Sec. 3 the forward computation scheme embodied by the pivotal Eqs. (21)–(23) is discussed in some detail for three particular applications, viz. the baffle step (Sec. 3.1), a simple source on a sphere (Sec. 3.2), and for the case that the cap velocity profile is a Stenzel-type profile (Sec. 3.3). A Stenzel profile is a certain type of smooth function of the elevation angle that vanishes at the rim of the cap to any desired degree. Section 4 provides the results for the power and directivity. In Sec. 5 the low-frequency limit for consideration of the acoustic center is discussed. The developments in Secs. 4–5, that apply to general symmetric velocity profiles, are illustrated using the two standard examples occurring in literature, viz. that of a uniformly moving cap in normal direction and in axial direction. The inverse problem, in which the expansion coefficients of the unknown profile are estimated from the measured pressure that the velocity profile gives rise to, is also feasible. This is largely due to the fact that the expansion terms are orthogonal and complete so that for smooth velocity profiles only a few coefficients are required. Combining the inverse method with the forward computation scheme of Sec. 2, it is seen that one can predict the acoustical quantities considered in Secs. 4–5 from a limited amount of measured pressure data. In the reverse direction, the inverse method can be used to design a velocity profile so as to meet certain specifications in the far field or near field of the radiator. While the theory necessary to do so is discussed in Sec. 6, this is not worked out further there. In Sec. 7 the extension of the methodology to non-axial symmetric profiles is briefly discussed. Finally, in Sec. 8 conclusions are presented.

2. BASIC FORMULAS

Assume a general velocity profile $V(\theta,\varphi)$ on a spherical cap, given in spherical coordinates as

$$S_0 = \{(r,\theta,\varphi) \mid r = R\,,\ 0 \le \theta \le \theta_0\,,\ 0 \le \varphi \le 2\pi\}\,, \tag{1}$$

with R the radius of the sphere with center at the origin and θ_0 the angle between the $z-$axis (elevation angle $\theta = 0$) and any line passing through the origin and a point on the rim of the cap. See Fig. 2 for the used geometry and notations. Thus it is assumed that V vanishes outside S_0. Furthermore, in loudspeaker applications, the cap moves parallel to the z-axis, and so $V(\theta,\varphi)$ will be identified with its z-component, and has normal component

$$W(\theta,\varphi) = V(\theta,\varphi)\cos\theta\,. \tag{2}$$

The average of this normal component over the cap,

$$\frac{1}{A_{S_0}} \iint_{S_0} W(\theta,\varphi)\sin\theta\,d\theta\,d\varphi\,, \tag{3}$$

is denoted by w_0, where A_{S_0} is the area of the cap, see Eq. (12). Then the time-independent part $p(r,\theta,\varphi)$ of the pressure due to a harmonic excitation of the membrane is given by

$$p(r,\theta,\varphi) = \\ -i\rho_0 c \sum_{n=-\infty}^{\infty} \sum_{m=-n}^{n} W_{mn}\, P_n^{|m|}(\cos\theta)\, \frac{h_n^{(2)}(kr)}{h_n^{(2)\prime}(kR)} e^{im\varphi}\,, \tag{4}$$

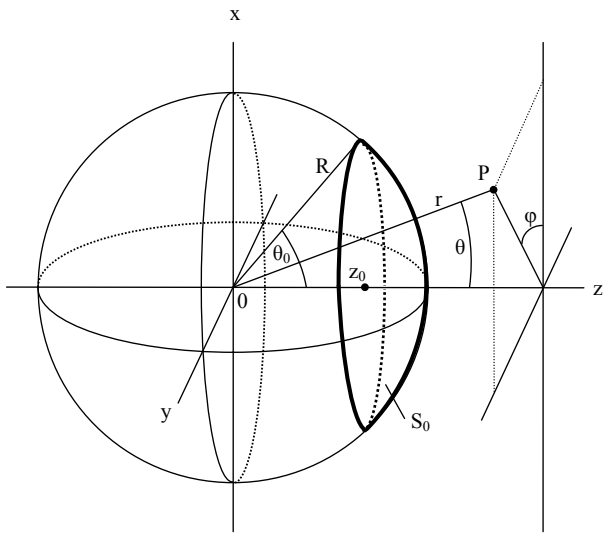

Fig. 2: Geometry and notations.

see Ref. [24, Ch. 7] or Ref. [25, Ch. 19] (Helmholtz equation with spherical boundary conditions). Here ρ_0 is the density of the medium, c is the speed of sound in the medium, $k = \omega/c$ is the wave number and ω is the radial frequency of the applied excitation, and $r \geq R$, $0 \leq \theta \leq \pi$, $0 \leq \varphi \leq 2\pi$. Furthermore, $P_n^{|m|}(\cos\theta)e^{im\varphi}$ is the spherical harmonic Y_n^m in exponential notation (compare with Ref. [24, Sec. 7.2], where sine-cosine notation has been used), $h_n^{(2)}$ is the spherical Hankel function, see Ref. [30, Ch. 10], of order n, and W_{mn} are the expansion coefficients of $W(\theta,\varphi)$, $0 \leq \theta \leq \pi$, $0 \leq \varphi \leq 2\pi$, relative to the basis $Y_n^m(\theta,\varphi)$. Thus

$$W(\theta,\varphi) = \sum_{n=-\infty}^{\infty} \sum_{m=-n}^{n} W_{mn} P_n^{|m|}(\cos\theta) \mathrm{e}^{im\varphi} \tag{5}$$

and

$$W_{mn} = \frac{n+1/2}{2\pi} \frac{(n-|m|)!}{(n+|m|)!} \int_0^{\pi} \int_0^{2\pi} W(\theta,\varphi)\, P_n^{|m|}(\cos\theta) e^{-im\varphi} \sin\theta \, d\theta \, d\varphi \, , \tag{6}$$

where it should be observed that the integration over θ in Eq. (6) is in effect only over $0 \leq \theta \leq \theta_0$ since V vanishes outside S_0.

In the case of axially symmetric velocity profiles V and W, written as $V(\theta)$ and $W(\theta)$, the right-hand sides of Eqs. (4) and (6) become independent of φ and simplify to [23, 24, 25]

$$p(r,\theta,\varphi) = -i\rho_0 c \sum_{n=0}^{\infty} W_n \, P_n(\cos\theta) \, \frac{h_n^{(2)}(kr)}{h_n^{(2)'}(kR)} \, , \tag{7}$$

and

$$W(\theta) = \sum_{n=0}^{\infty} W_n P_n(\cos\theta) \tag{8}$$

with

$$W_n = (n+1/2) \int_0^{\pi} W(\theta) \, P_n(\cos\theta) \sin\theta \, d\theta \, , \tag{9}$$

respectively, with P_n the Legendre polynomial of degree n. The integration in Eq. (9) is actually over $0 \leq \theta \leq \theta_0$. Since loudspeaker cones mainly vibrate in a radially symmetric fashion, almost all attention in this paper is limited to axially symmetric velocity profiles V and W. In Sec. 6 the generalization to non-axial symmetric profiles is briefly considered.

The case that W is constant w_0 on the cap S_0 has been treated in Ref. [23, Part III, Sec. 6], Ref. [24, p. 343], and Ref. [25, Sec. 20.5], with the result that

$$W_n = \frac{1}{2} w_0 (P_{n-1}(\cos\theta_0) - P_{n+1}(\cos\theta_0)) \, . \tag{10}$$

The pressure p is then obtained by inserting W_n into Eq. (7). Similarly, the case that V is constant v_0 on S_0 has been treated by Ref. [25, Sec. 20.6], with the result that

$$W_n = \tfrac{1}{2} v_0 \{ \tfrac{n+1}{2n+3} (P_n(\cos\theta_0) - P_{n+2}(\cos\theta_0)) + \tfrac{n}{2n-1} (P_{n-2}(\cos\theta_0) - P_n(\cos\theta_0)) \} \, . \tag{11}$$

In Eqs. (10) and (11) the definition $P_{-n-1} = P_n$, $n = 0, 1, \cdots$, has been used to deal with the case $n = 0$ in Eq. (10) and the cases $n = 0, 1$ in Eq. (11). In Fig. 1 the resemblance is shown between the polar plots of: a real driver in a rectangular cabinet (Fig. 1-a), a rigid piston in an infinite baffle (Fig. 1-b), and a rigid spherical cap in a rigid sphere (Fig. 1-c) using Eqs. (7) and (11). The driver (vifa MG10SD09-08, $a = 3.2$ cm) was mounted in a square side of a rectangular cabinet with dimensions 13x13x18.6 cm and measured on a turning table in an anechoic room at 1 m distance.

The area of a spherical cap is equal to

$$A_{S_0} = 4\pi R^2 \sin^2(\theta_0/2). \tag{12}$$

If this area is chosen to be equal to the area of the flat piston, there follows for the piston radius a that

$$a = 2R\sin(\theta_0/2). \tag{13}$$

The parameters used for Fig. 1 are $a = 3.2$ cm, $\theta_0 = \pi/8$, $R = 8.2$ cm, are such—using Eq. (13)—that the area of the piston and the cap are equal. The radius R of the sphere is such that the sphere and cabinet have comparable volumes, respectively 2.3 and 3.1 liters. If R is such that the sphere volume is the same as that of the cabinet, and θ_0 such that the area of the piston and the cap are equal, one gets $R = 9.0873$ cm and $\theta_0 = 0.35399$. The corresponding polar plot—not shown here—is very similar to Fig. 1-c, the deviations are about 1 dB or less. Apparently, the actual value of the volume is of modest influence. If we keep R fixed and change the cap area by changing the aperture θ_0 however, the influence can be significant. To illustrate this, polar plots are shown in Fig. 3 for constant V, using Eqs. (7) and (11). Figure 3 clearly shows that for increasing aperture until, say, $\theta_0 = \pi/2$, the radiation becomes more directive. However, in the limit case $\theta_0 = \pi$ there is only one non-zero W_n in Eqs. (10) and (11), viz. $W_n = \delta_{0n}$ for constant W and $W_n = \delta_{1n}$ for constant V (δ: Kronecker's delta), respectively. In the case of constant W this is a non-directive pulsating sphere. In the case of constant V we get

$$p(r,\theta) = -i\rho_0 c\, V \cos\theta \, \frac{h_1^{(2)}(kr)}{h_1^{(2)'}(kR)}\,, \tag{14}$$

plotted in Fig. 4. This case is discussed in Ref. [27, Sec. 4.-2] as the transversely oscillating rigid sphere. It is readily seen that $p(r,\theta)/p(r,0) = \cos\theta$.

It should be noted that the W_n in Eqs. (10) and (11) have poor decay, roughly like $n^{-1/2}$, and this shows that the representation of W through its Legendre coefficients is highly inefficient. While poor decay of W_n in Eq. (7) is not necessarily a problem for the forward problem (where the pressure p is computed from W using Eqs. (7) and (9)), it certainly is so for the inverse problem. In the inverse problem, one aims at estimating the velocity profile W (or V) from pressure measurements around the sphere. This can be done, in principle, by adopting a matching approach in Eq. (7) in which the W_n are optimized with respect to match of the measured pressure p

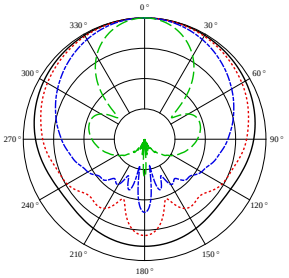

(a) θ_0 =$\pi/16$

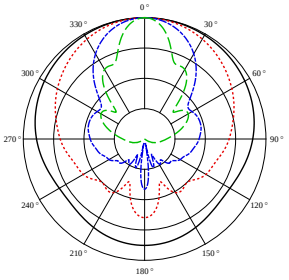

(b) θ_0 =$2\pi/16$

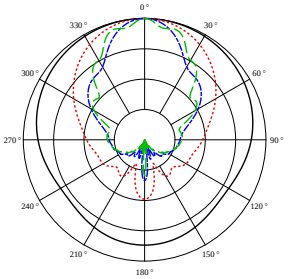

(c) θ_0 =$3\pi/16$

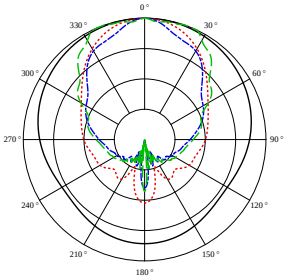

(d) θ_0 =$4\pi/16$

Fig. 3: Polar plots of the SPL (10 dB/div.), f= 1 kHz (solid curve), 4 kHz (dotted curve), 8 kHz (dashed-dotted curve), and 16 kHz (dashed curve), Rigid spherical cap for various aperture θ_0, (sphere radius $R = 8.2$ cm, $r = 1$ m) using Eqs. (7) and (11). All curves are normalized such that the SPL is 0 dB at θ=0.

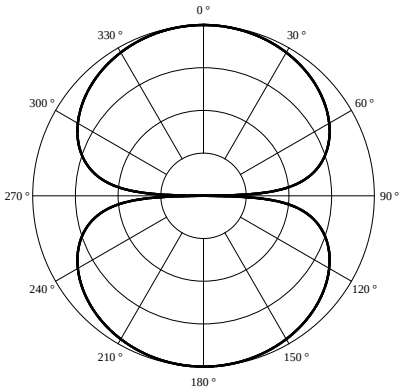

Fig. 4: Polar plot for a sphere ($\theta_0 = \pi$) moving with constant velocity V in the z-direction, using Eqs. (7) and (11). In this case $W_1 = 1$, W_n is equal to zero for all values $n \neq 1$.

and the theoretical expression for p in Eq. (7) involving the W_n. Even for the simplest case where W is constant, it is seen from the poor decay of the W_n and the poor decay of $P_n(\cos\theta)$ that a very large number of terms are required in the Legendre series in Eq. (8).

In this paper a more efficient representation of W is employed. This representation uses orthogonal functions on the cap that are derived from Zernike terms

$$R^0_{2\ell}(\rho) = P_\ell(2\rho^2 - 1) \ , \ \ 0 \le \rho \le 1 \ , \ \ \ell = 0, 1, \cdots \ , \tag{15}$$

that were also used in Refs.[18, 19, 20]. See, in particular, Ref. [20], Sec. 2 for motivation of this choice. Because of the geometry of the spherical cap, a variable transformation is required to pass from orthogonal functions $R^0_{2\ell}$ on the disk to orthogonal functions on the cap. In Ref. [20], Appendix A, it is shown that the functions

$$R^0_{2\ell}\Big(\frac{\sin\frac{1}{2}\theta}{\sin\frac{1}{2}\theta_0}\Big) \ , \ \ 0 \le \theta \le \theta_0 \ , \ \ \ell = 0, 1, \cdots \ , \tag{16}$$

are orthogonal on the cap. With

$$\theta = 2\arcsin(s_0\rho) \ ; \ s_0 = \sin\frac{1}{2}\theta_0 \ , \tag{17}$$

the inverse of the variable transformation used in Eq. (16), it follows then by orthogonality of the Zernike terms that

$$W(2\arcsin(s_0\rho)) = w_0 \sum_{\ell=0}^{\infty} u_\ell R^0_{2\ell}(\rho) \ , \ \ 0 \le \rho \le 1 \ , \tag{18}$$

where the expansion coefficients $w_0 u_\ell$ are given by

$$w_0 u_\ell = 2(2\ell + 1) \int_0^1 W(2\arcsin(s_0\rho)) R^0_{2\ell}(\rho) \rho d\rho \ . \tag{19}$$

It is this parametrization of W in terms of the expansion coefficients u_ℓ that will be preferred in the sequel. This parametrization is obtained by 'warping' W according to Eq. (17) and expanding the warped function as Eqs. (18)–(19) with s_0 as in Eq. (17).

The efficiency of the representation in Eq. (18) is apparent from the fact that a smooth profile W requires only a limited number of coefficients u_ℓ of relatively small amplitude yield an accurate approximation of $W(2\arcsin(s_0\rho))$. For instance, the constant profile $W = w_0$ on S_0 is represented exactly by only one term $w_0 R^0_0(\rho)$ in the expansion in Eq. (18), and the profile $W = v_0 \cos\theta$, corresponding to the case that V is constant v_0 on S_0, is represented exactly by two terms $v_0[(1-s_0^2)R^0_0(\rho) - s_0^2 R^0_2(\rho)]$. More complicated examples arise when V or W is a multiple of the Stenzel profile

$$(n+1)\Big(\frac{\cos\theta - \cos\theta_0}{1 - \cos\theta_0}\Big)^n \ , \tag{20}$$

and these require $n + 1$ terms in the representation in Eq. (18). These profiles vanish at the rim of S_0 to degree n and are considered in Sec. 3.3 and 6 to illustrate the methods developed in this paper.

It it shown [20] that the expansion in Eq. (18) gives rise to a series expression for the pressure p in the whole space outside and on the sphere. The main result is that for $r \ge R$, $\theta \in [0, \pi]$ and $\varphi \in [0, 2\pi]$

$$p(r, \theta, \varphi) = -i\rho_0 c w_0 \sum_{\ell=0}^{\infty} u_\ell S_\ell(r, \theta) \ , \tag{21}$$

where

$$S_\ell(r, \theta) = \sum_{n=\ell}^{\infty} (-1)^n s_0 (R^{2\ell+1}_{2n+1}(s_0) - R^{2\ell+1}_{2n-1}(s_0)) P_n(\cos\theta) \frac{h_n^{(2)}(kr)}{h_n^{(2)\prime}(kR)} \ , \tag{22}$$

in which

$$R_n^m(\rho) = \rho^m P_{\frac{n-m}{2}}^{(0,m)}(2\rho^2 - 1) \ , \qquad (23)$$

for integer $n, m \geq 0$ with $n - m$ even and ≥ 0 ($R_n^m \equiv 0$ otherwise) with $P_k^{(\alpha,\beta)}(x)$ the general Jacobi polynomial [30]. These polynomials $R_n^m(\rho)$ are called Zernike polynomials in optics [32, 33] and they were introduced recently in acoustics as well [18]. This main result provides the generalization of the forward computation scheme in Eqs. (7), (10), (11) to general axially symmetric velocity profiles W. Furthermore, it provides the basis for the inverse problem, in which the expansion coefficients u_ℓ are estimated from measured pressure data around the sphere by adopting a best match approach in Eq. (21). From these estimated coefficients an estimate of W can be made on basis of Eq. (18). The matter of convergence of the series in Eq. (22) and some computational issues are addressed elsewhere [20]. An alternative way [20] to calculate the pressure $p(r, \theta)$ is by using Eq. (7), where the W_n are now given by

$$W_n = (-1)^n s_0 w_0 \sum_{\ell=0}^{n} (R_{2n+1}^{2\ell+1}(s_0) - R_{2n-1}^{2\ell+1}(s_0)) u_\ell \ , \qquad (24)$$

rather than Eq. (9). This is particularly interesting for the forward computation scheme with velocity profiles that vanish smoothly at the rim of the cap as these require only a limited number of terms in Eq. (7).

3. APPLICATIONS OF THE MAIN RESULT

In this section the main result in Eqs. (21)–(23) is illustrated by considering three applications, viz. the baffle step, simple source on a sphere, and Stenzel velocity profiles.

3.1. Special case baffle step

At low frequencies the baffle of a loudspeaker is small compared to its wavelength and radiates due to diffraction effects in the full space (4π-field). At those low frequencies the radiator does not benefit from the baffle in terms of gain. At high frequencies the loudspeaker benefits from the baffle which yields a gain of 6 dB. This transition is the well-known baffle step. The center frequency of this transition depends on the size of the baffle. Olson [31] has documented this for twelve different loudspeaker enclosures, including the sphere, cylinder, and rectangular parallelepiped. All those twelve enclosures share the common feature of increasing gain by about 6 dB when the frequency is increased from low to high. The exact shape of this step depends on the particular enclosure. For spheres the transition is smoothest, while for other shapes undulations are manifest, in particular for cabinets with edgy boundaries. In Fig. 5 the baffle step is shown for a polar cap ($\theta_0 = \pi/8$) on a sphere of radius R=0.082 m using Eqs. (7) and (11), for different observation angles $\theta = 0$ (solid curve), $\theta = \pi/9$ (dotted curve), $\theta = 2\pi/9$ (dashed-dotted curve), and $\theta = 3\pi/9$ (dashed curve). Compare the curves of Fig. 5 with the measurements using the experimental loudspeaker discussed in Sec. 2. It appears that there is a good resemblance between the measured frequency response of the experimental loudspeaker. The undulations, e.g., for $\theta = 3\pi/9$ (dashed curve) at 7.4, 10, and 13.4 kHz correspond well. Although these undulations are often attributed to the non-rigid cone movement of the driver itself, our pictures show that it is mainly a diffraction effect. Furthermore, it can be observed that even on-axis ($\theta = 0$) there is a gradual decrease of SPL at frequencies above about 10 kHz. It can be shown from the asymptotics of the spherical Hankel functions that for $\theta = 0$, $k \to \infty$, and $r \gg R$, the sound pressure $p(r, \theta)$ given by Eq. (21) decays at least as $\mathrm{O}(k^{-1/3})$. This is in contrast with a flat piston in an infinite baffle. There, the on-axis pressure does not decay. This is discussed further at the end of Sec. 4.1.

3.2. Special case W is a simple source on S_0

If the polar cap aperture θ_0 decreases towards 0, the cap acts as a simple source. It follows from Eqs. (21)–(23) and by proper normalization by the cap area A_{S_0}, using Eq. (12), and the definition of w_0 in Eq. (3), that

$$p(r, \theta, \varphi) = -i\rho_0 c w_0 \sum_{n=0}^{\infty} (2n+1) P_n(\cos\theta) \, \frac{h_n^{(2)}(kr)}{h_n^{(2)'}(kR)} \ . \qquad (25)$$

In Fig. 6 the corresponding polar plot is illustrated, where the same sphere radius and frequencies are used as in Fig. 1-c. It appears that the difference between the response at θ=0 and π is not large, especially for low frequencies. This is discussed further in Sec. 5 with regard to the acoustic center.

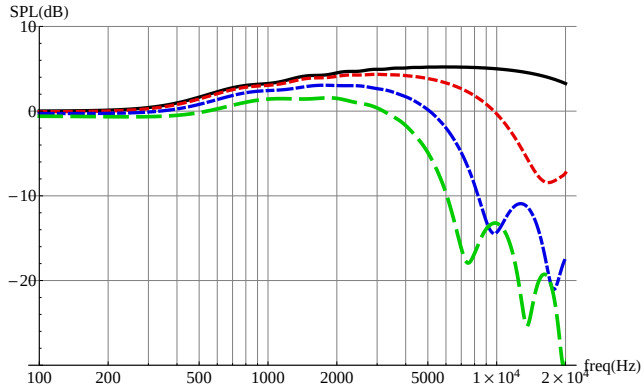

(a)

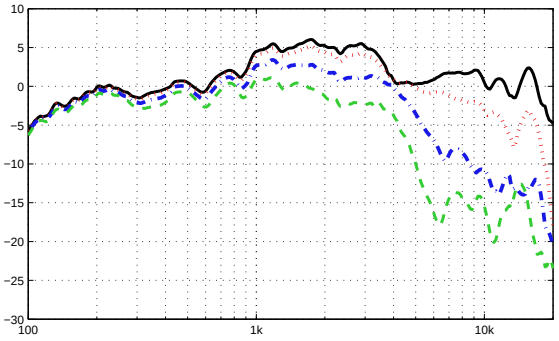

(b)

Fig. 5: (a) Baffle step of a polar cap ($\theta_0 = \pi/8$) on a sphere of radius R =0.082 m, $\theta = 0$ (solid curve), $\theta = \pi/9$ (dotted curve), $\theta = 2\pi/9$ (dashed-dotted curve), and $\theta = 3\pi/9$ (dashed curve), at distance $r = 1$ m, using Eqs. (21)–(23). All curves are normalized such that the SPL is 0 dB at 100 Hz. (b) Frequency response of a driver (same as Fig. 1-a, $a = 3.2$ cm) mounted in a square side of a rectangular cabinet with dimensions 13x13x18.6 cm, where the parameter is the observation angle θ. The loudspeaker was measured in an anechoic room at 1 m distance. The on-axis response was normalized to 0 dB at 200 Hz, the other curves were normalized by the same amount.

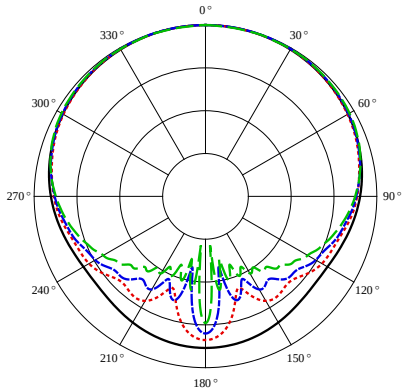

Fig. 6: Polar plots of the SPL (10 dB/div.) of a simple source on a sphere of radius R =0.082 m. Frequency $f = 1$ kHz (solid curve), 4 kHz (dotted curve), 8 kHz (dashed-dotted curve), and 16 kHz (dashed curve), at distance $r = 1$ m, using Eqs. (25). All curves are normalized such that the SPL is 0 dB at θ=0.

3.3. Stenzel-type profiles and forward computation

Consider the profile

$$V^{(K)}(\theta) = v_0^{(K)}(K{+}1)\Big(\frac{\cos\theta - \cos\theta_0}{1-\cos\theta_0}\Big)^K \ , \ 0 \le \theta \le \theta_0 \ , \tag{26}$$

with $V^{(K)}(\theta) = 0$ for $\theta_0 < \theta \le \pi$ (as usual), $K = 0, 1, \cdots$. Then a simple computation shows that

$$V^{(K)}(2\arcsin(s_0\rho)) = v_0^{(K)}(K{+}1)(1{-}\rho^2)^K \ , 0 \le \rho \le 1 \ . \tag{27}$$

The right-hand side of Eq. (27) is the Stenzel profile, considered extensively in Ref. [18]. Thus

$$V^{(K)}(2\arcsin(s_0\rho)) = v_0^{(K)} \sum_{\ell=0}^{K} q_\ell^{(K)} R_{2\ell}^0(\rho) \ , \ 0 \le \rho \le 1 \ , \tag{28}$$

where

$$q_\ell^{(K)} = (K+1)(-1)^\ell \, \frac{2\ell+1}{\ell+1} \, \frac{\binom{K}{\ell}}{\binom{K+\ell+1}{K}} \ , \tag{29}$$

$\ell = 0, 1, \cdots, K$.

From

$$W^{(K)}(\theta) = V^{(K)}(\theta)\cos\theta = \frac{K+1}{K+2}(1-\cos\theta_0)V^{(K+1)}(\theta) + (\cos\theta_0)V^{(K)}(\theta)\ , \tag{30}$$

it follows that

$$W^{(K)}(2\arcsin(s_0\rho)) = w_0^{(K)}\sum_{\ell=0}^{K+1} u_\ell^{(K)} R_{2\ell}^0(\rho)\ ,$$
$$0 \le \rho \le 1\ , \tag{31}$$

where

$$w_0^{(K)} = \frac{K+1+\cos\theta_0}{K+2} v_0^{(K)} \quad , \tag{32}$$

and, for $\ell = 0, 1, \cdots, K+1$,

$$u_\ell^{(K)} = \frac{v_0^{(K)}}{w_0^{(K)}}\left[\frac{K+1}{K+2}(1-\cos\theta_0)q_\ell^{(K+1)} + (\cos\theta_0)q_\ell^{(K)}\right]. \tag{33}$$

Thus one can compute the pressure using the formulas in Eqs. (21)–(23) with $u_\ell = u_\ell^{(K)}$.

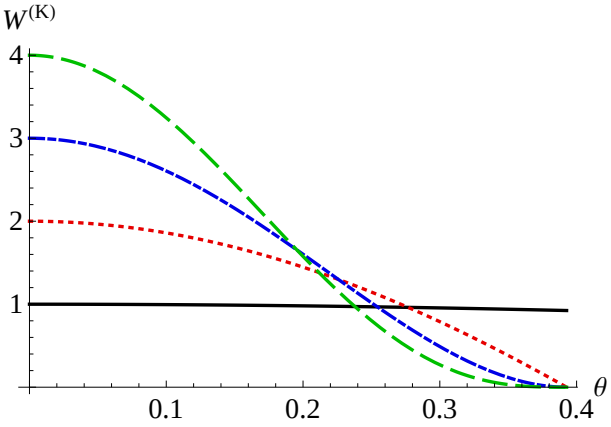

Fig. 7: Stenzel profiles for K=0 (solid curve), K=1 (dotted curve), K=2 (dashed-dotted curve), and K=3 (dashed curve), using Eqs. (26) and (30) and $\theta_0 = \pi/8$.

In Fig. 7 Stenzel profiles are plotted for K=0 (solid curve), K=1 (dotted curve), K=2 (dashed-dotted curve), and K=3 (dashed curve). In Fig. 8 polar plots are displayed of the SPL (10 dB/div.) of a spherical cap ($\theta_0 = \pi/8$, $R = 8.2$ cm, $r = 1$ m) with various Stenzel velocity profiles, K=0 (solid curve), K=1 (dotted curve), K=2 (dashed-dotted curve), and K=3 (dashed curve), (a) f = 4 kHz, (b) f = 8 kHz. It appears that the difference between the various velocity profiles are more pronounced at higher frequencies. Also, the cap becomes less directive for higher K values because in the limit $K \to \infty$ it would behave like a simple source on a sphere. Furthermore, it appears that the solid curves ($K = 0$) for (a) f = 4 kHz and (b) f = 8 kHz are the same as the dotted and dashed-dotted curves, respectively in Fig. 1-c. Note that Figs. 1-c and 8 were produced using two different sets of formulas, viz. Eqs. (7) and (11) for Fig. 1-c and Eqs. (21) and (33) for Fig. 8, and that they yield the same plots.

4. POWER AND DIRECTIVITY

The power is defined as the intensity pv^* integrated over the sphere S_r of radius $r \ge R$,

$$P = \int_{S_r} pv^* dS_r\ , \tag{34}$$

where p and v are the pressure and velocity at an arbitrary point on the sphere. Using Eq. (7) for the pressure and

$$v = \frac{-1}{ik\rho_0 c}\frac{\partial p}{\partial \underline{n}} \tag{35}$$

we get

$$v(r,\theta,\varphi) = \sum_{n=0}^{\infty} W_n\, P_n(\cos\theta)\, \frac{h_n^{(2)'}(kr)}{h_n^{(2)'}(kR)}\ . \tag{36}$$

By the orthogonality of the Legendre polynomials it follows that

$$P = \int_{S_r} pv^* dS_r = 2\pi\int_0^\pi p(r,\theta)v^*(r,\theta)r^2\sin\theta d\theta = -i\rho_0 c\sum_{n=0}^{\infty}\frac{|W_n|^2}{n+1/2}\frac{2\pi r^2 h_n^{(2)'}(kr)(h_n^{(2)'}(kr))^*}{|h_n^{(2)'}(kR)|^2}\ . \tag{37}$$

Using Ref. [30], Eq. 10.1.6,

$$\mathcal{W}\{j_n(z), y_n(z)\} = j_n(z)y_n'(z) - j_n'(z)y_n(z) = \frac{1}{z^2}, \tag{38}$$

where $\mathcal{W}$ in Eq. (38) denotes the Wronskian, we get

$$\Re[P] = \frac{2\pi\rho_0 c}{k^2}\sum_{n=0}^{\infty}\frac{|W_n|^2}{(n+1/2)|h_n^{(2)'}(kR)|^2}\ . \tag{39}$$

Note that Eq. (39) has been derived without using any (near-field or far-field) approximation. The

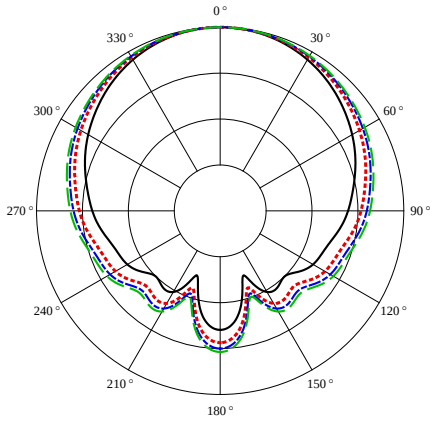

(a)

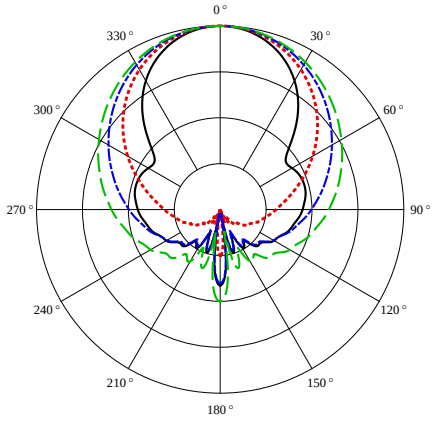

(b)

Fig. 8: Polar plots of the SPL (10 dB/div.) of a spherical cap ($\theta_0 = \pi/8$, $R = 8.2$ cm, $r = 1$ m) with various Stenzel velocity profiles, K=0 (solid curve), K=1 (dotted curve), K=2 (dashed-dotted curve), and K=3 (dashed curve). (a) f = 4 kHz, (b) f = 8 kHz. All curves are normalized such that the SPL is 0 dB at θ=0.

real part of the acoustical power is independent of r, which is in accordance with the conservation of power law. For low frequencies Eq. (39) is approximated as

$$\Re[P] = 4\pi\rho_0 c W_0^2 k^2 R^4 \,. \tag{40}$$

To illustrate Eq. (39), the normalized power $\frac{\Re[P]}{2\pi\rho_0 c v_0^2 R^2}$ is plotted in Fig. 9, where a cap with various apertures, $\theta_0 = 5\pi/32$ (solid curve), $\theta_0 = \pi/8$ (dotted curve), and $\theta_0 = \pi/10$ (dashed-dotted curve) is moving with a constant velocity v_0 (using Eq. (10)).

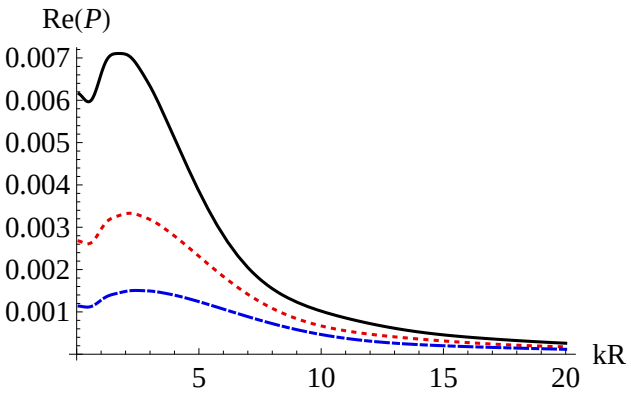

Fig. 9: The power $\frac{\Re[P]}{2\pi\rho_0 c v_0^2 R^2}$ of a rigid spherical cap moving with a constant velocity v_0 and various apertures, $\theta_0 = 5\pi/32$ (solid curve), $\theta_0 = \pi/8$ (dotted curve), and $\theta_0 = \pi/10$ (dashed-dotted curve), sphere radius $R = 8.2$ cm using Eqs. (10) and (39).

Next, we compare the calculated power with the power measured in a reverberation room using the experimental loudspeaker discussed in Sec. 2. Here we assumed the pole cap moving with a constant acceleration ($a_0 = ikcv_0$)—corresponding with a frequency independent current of a constant amplitude through the loudspeaker. Figure 10 shows plots of the calculated power for a rigid spherical cap moving with a constant acceleration and various apertures, $\theta_0 = 5\pi/32$ (solid curve), $\theta_0 = \pi/8$ (dotted curve), and $\theta_0 = \pi/10$ (dashed-dotted curve), together with the power obtained from the measured loudspeaker (dashed-irregular curve). It appears that the calculated power for $\theta_0 = \pi/8$ (dotted curve) and the power from the measured loudspeaker (dashed-irregular curve) are quite similar,

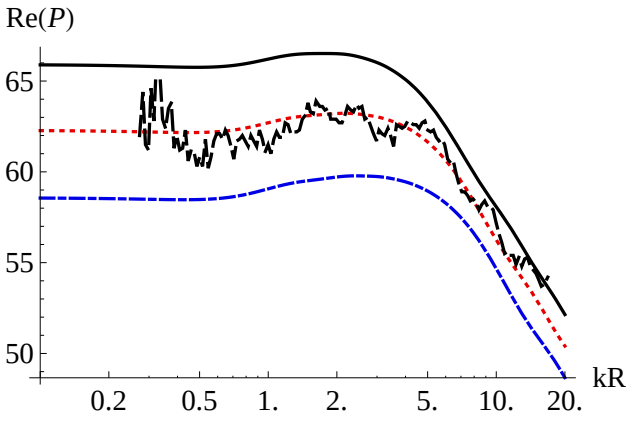

Fig. 10: The power $\frac{\Re[P]c}{2\pi\rho_0 a_0^2 R^4}$ [dB] vs. kR (log. axis) of a rigid spherical cap moving with a constant acceleration and various apertures, $\theta_0 = 5\pi/32$ (solid curve), $\theta_0 = \pi/8$ (dotted curve), and $\theta_0 = \pi/10$ (dashed-dotted curve), sphere radius $R = 8.2$ cm using Eqs. (10) and (39), together with power from the measured loudspeaker (dashed-irregular curve). The logarithmic horizontal axis runs from kR=0.1–20, corresponding to a frequency range from 66 Hz–13.2 kHz.

while there was no special effort done to obtain a best fit. A slightly larger aperture than the 'round' value $\theta_0 = \pi/8$, which we use in many examples in the paper, would have resulted in a better fit. The low-frequency behavior of Fig. 10 follows directly by multiplying Eq. (40) with $1/(kc)^2$ because of the constant acceleration of the cap.

4.1. Directivity

The far-field pressure can be calculated by substituting the asymptotic value [30, Ch. 10]

$$h_n^{(2)}(kr) \approx i^{n+1}\frac{\mathrm{e}^{-ikr}}{kr} \tag{41}$$

in Eq. (7), which leads to

$$p(r,\theta) \approx \rho_0 c \frac{\mathrm{e}^{-ikr}}{kr}\sum_{n=0}^{\infty}\frac{i^n W_n}{h_n^{(2)'}(kR)}P_n(\cos\theta)\ . \tag{42}$$

In Kinsler et al. [26, Sec. 8.9], the far-field relation is written as

$$p(r,\theta,\varphi) = p_{ax}(r)H(\theta,\varphi), \tag{43}$$

in which $p_{ax}(r)$ is the pressure at $\theta = 0$, and $H(\theta,\varphi)$ is dimensionless with $H(0,0)$=1. Since there is no φ dependence, we delete it. This leads to

$$p_{ax}(r) = \rho_0 c \frac{\mathrm{e}^{-ikr}}{kr}\sum_{n=0}^{\infty}\frac{i^n W_n}{h_n^{(2)'}(kR)}\ , \tag{44}$$

and

$$H(\theta) = \frac{p(r,\theta)}{p_{ax}(r)} = \frac{\sum_{n=0}^{\infty}\frac{i^n W_n}{h_n^{(2)'}(kR)}P_n(\cos\theta)}{\sum_{n=0}^{\infty}\frac{i^n W_n}{h_n^{(2)'}(kR)}}. \tag{45}$$

The total radiated power Π in the far field follows from Eq. (34) and the far-field relation $v = p/(\rho_0 c)$ as

$$\Pi = \int_{S_r}\frac{1}{\rho_0 c}|p|^2 dS_r = \frac{1}{\rho_0 c}|p_{ax}(r)|^2 r^2\int_0^{2\pi}\int_0^{\pi}|H(\theta,\varphi)|^2\sin\theta\,d\theta\,d\varphi\ . \tag{46}$$

For a simple (non-directive) source at the origin to yield the same acoustical power on S_r, the pressure p_s should satisfy

$$\Pi = \frac{1}{\rho_0 c}4\pi r^2|p_s(r)|^2\ . \tag{47}$$

Therefore, the directivity defined as

$$D = |p_{ax}(r)|^2/|p_s(r)|^2 \ , \qquad (48)$$

follows from Eqs. (46) and (47), using the orthogonality of the Legendre polynomials, as

$$D = \frac{2|\sum_{n=0}^{\infty} \frac{i^{n+1}W_n}{h_n^{(2)'}(kR)}|^2}{\sum_{n=0}^{\infty} \frac{|W_n|^2}{(n+1/2)|h_n^{(2)'}(kR)|^2}} \ . \qquad (49)$$

The directivity index $DI = 10\log_{10} D$ [dB] vs. kR is plotted in Fig. 11. For comparison the directivity

$$D_{rp} = \frac{(ka)^2}{1 - J_1(2ka)/ka} \qquad (50)$$

of a rigid piston in an infinite baffle [26] is plotted in Fig. 11 (with $ka = kR/2.5$, so that the $\pi/8$-cap and piston have the same area), as the light-long-dashed curve starting at 3 dB. At low frequencies the directivity D_{rp} is 3 dB because the piston is radiating in the 2π-field, while the caps are radiating in the 4π-field. At higher frequencies the curve almost coincides with the dotted curve which corresponds to the $\theta_0 = \pi/8$ cap.

Now consider the case that $kR \to \infty$. Then using $h_n^{(2)'}(kR) \approx i^n \mathrm{e}^{-ikR}/kR$, it follows that D is approximated by

$$D \approx \frac{2|\sum_{n=0}^{\infty} W_n|^2}{\sum_{n=0}^{\infty} \frac{|W_n|^2}{(n+1/2)}} = \frac{2|W(\theta=0)|^2}{\int_0^{\pi} |W(\theta)|^2 \sin\theta d\theta}, \qquad (51)$$

or, in words, by the ratio of $|W(\theta = 0)|^2$ and the average value of $|W(\theta)|^2$ over the sphere. Equations (49) and (51) show that the directivity—which is a typical far-field acoustical quantity—is fully determined in a simple manner by the velocity profile of the pole cap, which can be easily derived from measurements, e.g., with a laser-Doppler meter. This procedure is not elaborated here. A similar result was obtained for a flexible radiator in an infinite flat baffle [19]. In the flat baffle case the directivity increases with $(ka)^2$. For the cap case, there is indeed an initial increase with $(kR)^2$, but at very high frequencies, there is a decrease of the directivity. These high frequencies are in most cases out of the audio range, but may be of importance for ultrasonics. The deviation of the $(kR)^2$-behavior appears in Fig. 11 for θ_0 as low as $5\pi/32$ (solid curve).

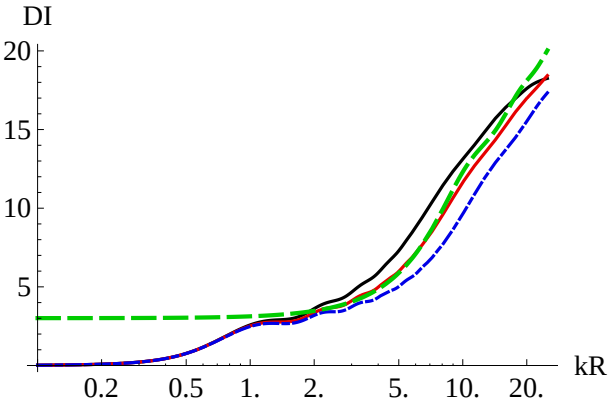

Fig. 11: The directivity index $DI = 10\log_{10} D$ [dB] vs. kR (log. axis) of a rigid spherical cap with various apertures, $\theta_0 = 5\pi/32$ (solid curve), $\theta_0 = \pi/8$ (dotted curve), and $\theta_0 = \pi/10$ (dashed-dotted curve), and sphere radius $R = 8.2$ cm using Eqs. (10) and (49). The light-long-dashed curve starting at 3 dB is the directivity for a rigid piston in an infinite baffle, using Eq. (50). The logarithmic horizontal axis runs from kR=0.1–25, corresponding to a frequency range from 66 Hz–16.5 kHz.

This effect may seem counterintuitive or even non-physical, however, the on-axis ($\theta = 0$) pressure decreases for high frequencies as well (see Fig. 5). This will decrease the numerator in Eq. (48) of the directivity. This effect does not occur with a piston in an infinite baffle, which has a constant, non-decreasing on-axis sound pressure, but a narrowing beam width.

5. THE ACOUSTIC CENTER

The acoustic center of a reciprocal transducer can be defined as the point from which spherical waves seem to be diverging when the transducer is acting as a source. There are more definitions, however, see Ref. [34] for an overview and discussion. This concept is mainly used for microphones. Recently, the acoustic center was elaborated [35] for normal sealed-box loudspeakers as a particular point that acts as the origin of the low-frequency radiation of the loudspeaker. At low frequencies, the radiation from such a loudspeaker becomes simpler as the wavelength of the sound becomes larger relative to the enclosure dimensions, and the system behaves externally as a simple source (point source). The difference from the origin to the true acoustic center

is denoted as Δ. If $p(r,0)$ and $p(r,\pi)$ are the sound pressure in front and at the back of the source, respectively, then Δ follows from

$$\frac{|p(r,0)|}{r+\Delta} = \frac{|p(r,\pi)|}{r-\Delta}\,, \tag{52}$$

as

$$\Delta = r\frac{|q|-1}{|q|+1}, \tag{53}$$

where

$$q = p(r,0)/p(r,\pi). \tag{54}$$

The pole-cap model is used to calculate the function q via Eq. (7), see Fig. 12. Subsequently, this model is used to compute the acoustic center with Eq. (53). Assume that $kR \ll 1$ and $R/r \ll 1$, and also that W_n is real with W_n of at most the same order of magnitude as W_0. Then two terms of the series in Eq. (7) are sufficient, and using $P_n(1) = 1$ and $P_n(-1) = (-1)^n$, q can be written as

$$q \approx \Big(W_0\,\frac{h_0^{(2)}(kr)}{h_0^{(2)'}(kR)} + W_1\,\frac{h_1^{(2)}(kr)}{h_1^{(2)'}(kR)}\Big)\Big/ \Big(W_0\,\frac{h_0^{(2)}(kr)}{h_0^{(2)'}(kR)} - W_1\,\frac{h_1^{(2)}(kr)}{h_1^{(2)'}(kR)}\Big). \tag{55}$$

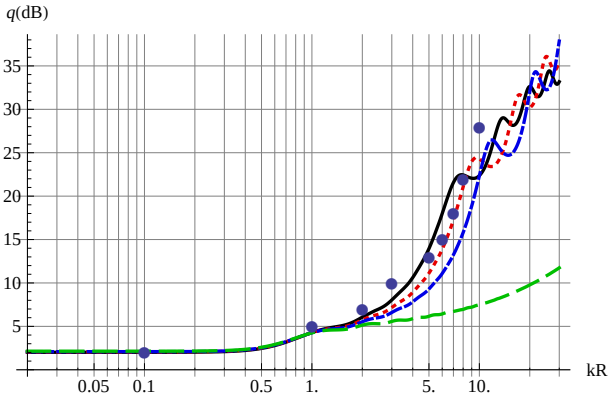

Fig. 12: The function $20\,\log_{10}|q|$ [dB] vs. kR (log. axis) given by Eq. (54) of a rigid spherical cap with various apertures, $\theta_0 = 5\pi/32$ (solid curve), $\theta_0 = \pi/8$ (dotted curve), and $\theta_0 = \pi/10$ (dashed-dotted curve), using Eqs. (7) and (11), and a simple source on a sphere using Eq. (25) (dashed curve), all at $r =$ 1 m and sphere radius $R = 8.2$ cm. The solid circles are from a real driver (same as Fig. 1-a, $a = 3.2$ cm) mounted in a square side of a rectangular cabinet. The logarithmic horizontal axis runs from kR=0.02–30, corresponding to a frequency range from 13 Hz–19.8 kHz.

Because $kR \ll 1$, the small argument approximation of the spherical Hankel functions

$$h_0^{(2)'}(z) \approx \frac{-i}{z^2},\; h_1^{(2)'}(z) \approx \frac{-2i}{z^3}, \tag{56}$$

can be used, and together with the identity

$$\frac{h_1^{(2)}(kr)}{h_0^{(2)}(kr)} = \frac{1}{kr}(1+ikr)\,, \tag{57}$$

we get

$$q \approx \Big(1+\frac{W_1}{2W_0}(1+ikr)\frac{R}{r}\Big)\Big/\Big(1-\frac{W_1}{2W_0}(1+ikr)\frac{R}{r}\Big)\,. \tag{58}$$

By our assumptions we have $|\frac{W_1}{2W_0}(1+ikr)\frac{R}{r}| \ll 1$ and so

$$q \approx 1+\frac{W_1}{W_0}\frac{R}{r}(1+ikr)\,. \tag{59}$$

Finally, assuming that $(kr)^2 \ll 2|\frac{W_0}{W_1}|\frac{r}{R}$, there holds

$$|q| \approx 1+\frac{W_1}{W_0}\frac{R}{r}\,, \tag{60}$$

and if $\frac{W_1 R}{W_0 r} \ll 1$ there holds

$$\varphi_q = \arg q \approx \arctan\frac{W_1}{W_0}\frac{\omega R}{c}\,, \tag{61}$$

where it has been used that W_1/W_0 is real and $k = \omega/c$. Substitution of Eq. (60) into Eq. (53) results in

$$\Delta \approx \frac{R\,W_1}{2\,W_0}\,. \tag{62}$$

Note that this result is real, independent of k and r, and only mild assumptions were used. The delay between the front and at the back of the source is equal to $\tau = d\varphi_q/d\omega$. Using Eqs. (61) and (62), and assuming $kR \ll \frac{W_0}{W_1}$ we get

$$\tau \approx \frac{2\Delta}{c}\,. \tag{63}$$

For the case W is constant the W_n follow from Eq. (10) resulting in

$$\Delta \approx \frac{3}{4}R(1+\cos\theta_0)\,. \tag{64}$$

If $\theta_0 = \pi$ and W is constant, the radiator is a pulsating sphere, and has according to Eq. (64) its acoustical center at the origin. For the case V is constant the W_n follow from Eq. (11) resulting in

$$\Delta \approx R\big(\cos\theta_0 + \frac{1}{1+\cos\theta_0}\big)\,. \tag{65}$$

If $\theta_0 = \pi$ and V is constant, the notion of acoustical center does not make sense, because of the notches in the polar plot at low frequencies, see Fig. 4. The absolute error in the approximation of Δ/R by Eq. (65) (for f=1 Hz, R=8.2 cm, r=100 m, and $0 \le \theta_0 \le \pi/2$) is $< 5\,10^{-7}$. Figure 12 shows that for that case the low-frequency asymptote is flat to about $kR = 0.4$ corresponding to 264 Hz. Hence the approximation of Δ/R by Eq. (65) is rather accurate up to this frequency. The relative acoustic center difference Δ/R vs. θ_0 is plotted in Fig. 13 for W is constant (solid curve) and V is constant (dotted curve), using Eqs. (64) and (65), respectively. Note that Δ/R=3/2 for $\theta_0 = 0$ in both cases that V and W are constant. This agrees with what would be given by the simple source on a sphere, see Sec. 3.2. This follows also from Eq. (25): we have W_0=1 and W_1=3, and by Eq. (62) we obtain Δ/R=3/2. This is for low frequencies also shown in Ref. [34, Fig. 3, Eqs. 18–19]. Further, it appears that for modest apertures, say $\theta_0 \le 0.5$ the difference between the right-hand sides of Eqs. (64) and (65) is very small and is of $\mathrm{O}(\theta_0^4)$. From this we may conclude that—at low frequencies ($kR \le 0.4$)—the acoustic center for a loudspeaker lies about 0–0.5 R in front of the loudspeaker, where R is the radius in the case of a spherical cabinet, or some other dimensional measure of the cabinet. At higher frequencies the acoustic center shifts further away from the loudspeaker. For example between kR=1 (660 Hz) and kR=2 (1.32 kHz), q is about 5 dB (see Fig. 12) corresponding (using Eq. (53)) to $\Delta = 3.4R = 28$ cm.

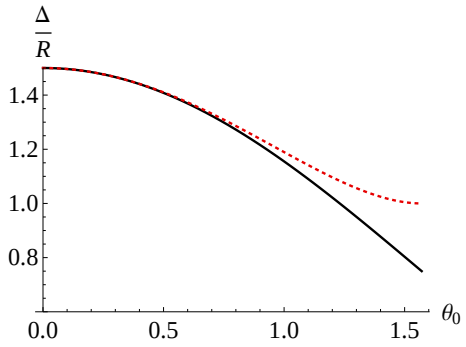

Fig. 13: The relative acoustic center difference Δ/R vs. θ_0 using Eq. (64) for W is constant (solid curve) and using Eq. (65) for V is constant (dotted curve).

The polar response $|p(r,\theta)/p(r,0)|$ at low frequencies can be computed in a similar way as q in Eq. (58). The minus sign in the denominator at the right-hand side of Eq. (58) is due to $P_1(\cos\pi) = -1$. Using now $P_1(\cos\theta) = \cos\theta$ and interchanging the numerator and denominator of Eq. (58) yields

$$\frac{p(r,\theta)}{p(r,0)} \approx \left(1 + \frac{W_1}{2W_0}(1+ikr)\frac{R}{r}\cos\theta\right) \Big/ \left(1 + \frac{W_1}{2W_0}(1+ikr)\frac{R}{r}\right). \tag{66}$$

Assuming that $(kr)^2 \ll 2|\frac{W_0}{W_1}|\frac{r}{R}$, Eq. (66) can be approximated by

$$\left|\frac{p(r,\theta)}{p(r,0)}\right| \approx 1 + (\cos\theta - 1)\frac{W_1}{2W_0}\,\frac{R}{r}. \tag{67}$$

Equation (67) clearly shows that the deviation from omni-directional radiation is proportional to the ratios $W_1/2W_0$ and R/r, while it is independent of the frequency for low frequencies. For fixed $W_1/2W_0$ and R/r the polar pattern is not truly omni-directional at low frequencies. This is because the acoustic center does not coincide with the origin in general .

6. INVERSE PROBLEM

The Eqs. (21)–(23) show how to compute the pressure in the space $r \ge R$ due to a harmonically excited (wave number k) membrane on the spherical cap $0 \le \theta \le \theta_0$ with a known radial component W of a velocity profile. In the reverse direction, the Eqs. (21)–(23) can serve as the basis for a method for estimating W from measurements of the pressure p in the space $r \ge R$ that W gives rise to. This yields a method for far-field loudspeaker assessment from near-field data (generalized Keele scheme) see [18] where this was applied to predict far-field sound pressure data from near-field measured pressure data. Because the pressure data can be collected in the (relative) near-field of a loudspeaker, this avoids the use of anechoic rooms that would be necessary if the far-field were to be assessed directly. The profile W can usually be estimated accurately by a limited number of expansion coefficients u_ℓ in Eq. (18), and these can be estimated by taking a matching approach in Eq. (22) in which the u_ℓ are chosen such that they optimize the match between the measured pressure and the theoretical

expression involving the u_ℓ at the right-hand side of Eq. (22). Given measurements, see Fig. 1,

$$\hat{p_j} = \hat{p_j}(P_j)\ , P_j = r_j(\cos\varphi_j \sin\theta_j, \sin\varphi_j \sin\theta_j, \cos\theta_j)\ , \tag{68}$$

where $j = 0, 1, \cdots, J$, the numbers $d_\ell, \ell = 0, 1, \cdots, L$, are chosen such that

$$\sum_{j=0}^{J} |\hat{p}_j - \sum_{\ell=0}^{L} d_\ell S_\ell(r_j, \theta_j)|^2 \sin\theta_j\ , \tag{69}$$

is minimal. The solution of this minimization problem can be obtained by standard linear algebra methods. Then $w_0\,, u_\ell\,, \ell = 0, 1, \cdots, L$ are estimated by setting

$$d_0 = -i\rho_0 c w_0\ , u_\ell = d_\ell/d_0\ ,\ \ell = 0, 1, \cdots, L\,. \tag{70}$$

There are various questions that arise in connection with the above optimization problem, such as number and choice of the measurement points P_j, choice of L, condition of the linear systems that occur, influence of noise and of systematic errors (such as incorrect setting of R and/or θ_0), etc. It is out of the scope of the present paper to address any of these issues in detail. Instead, one representative simulation example is given.

Simulation example

Take $R = 8.2$ cm, $\theta_0 = \pi/4$, $k = \omega/c = 2\pi f/c$ with $c = 340$ m/s, f= 4 kHz, so that $kR = 6$. The measurement points $P_j(r_j, \theta_j, \varphi_j)$ are taken in the form

$$\begin{aligned} &R\,2^{j_1/J_1} = r(j_1)\ ,\ \frac{\pi(j_2 - \frac{1}{2})}{J_2} = \theta(j_2)\ , \\ &\frac{2\pi(j_3 - \frac{1}{2})}{J_3} = \varphi(j_3)\ , \end{aligned} \tag{71}$$

with $j_1 = 1, \cdots, J_1 = 4$; $j_2 = 1, \cdots, J_2 = 6$; $j_3 = 1, \cdots, J_3 = 6$. Such a set of measurement points yields a convenient implementation of the solution of the optimization problem but does not need to be optimal in any other respect (not aimed at here, as said). The profile W is chosen to be

$$W^{(K)}(\theta) = V^{(K)}(\theta)\cos\theta\ ,\ 0 \le \theta \le \theta_0\ , \tag{72}$$

where $V^{(K)}(\theta)$ is the K^{th} Stenzel-type profile as in Sec. 3.3 (see Eqs. (26), (30)), and $K = 2$. We require for this example $v_0 = v_0^{(K)} = 1$ m/s, and by Eqs. (32) and (33) we get respectively $w_0 = w_0^{(K)}$ and

$$\begin{aligned} u_\ell^{(K)} = &\frac{K+2}{K+1+\cos\theta_0}\big[\frac{K+1}{K+2}(1-\cos\theta_0)q_\ell^{(K+1)} + \\ &(\cos\theta_0)q_\ell^{(K)}\big]. \end{aligned} \tag{73}$$

Using $q_\ell^{(K+1)}$, $q_\ell^{(K)}$ given by Eq. (29), the pressure p is computed in accordance with Eq. (21) with $u_\ell = u_\ell^{(K)}$. Measurements $\hat{p_j}$ are obtained in simulation by adding complex white noise (SNR= 40 dB) to the computed $p(P_j)$. The non-zero coefficients of $W^{(K)}$ are estimated by taking $L = K + 1$ in the optimization problem, and this yields estimates $\hat{w_0}$, $\hat{u}_0$, $\cdots$, $\hat{u}_{K+1}$ of w_0, u_0, $\cdots$, u_{K+1}. Figure 14 for the case K=2 shows the Stenzel profile $W^{(K)}$ of Eq. (72) using Eq. (20) directly (solid curve) together with the reconstructed profiles

$$\hat{W}^{(K)}(\theta) = \hat{w}_0^{(K)} \sum_{\ell=0}^{K+1} \hat{u}_\ell R_{2\ell}^0\Big(\frac{\sin\frac{1}{2}\theta}{\sin\frac{1}{2}\theta_0}\Big)\ ,\ 0 \le \theta \le \theta_0\ , \tag{74}$$

without noise (dotted curve) and with noise (dashed-dotted curve) added to the pressure points $\hat{p_j}$. The recovered $\hat{u}_\ell$ are computed by solving Eq. (69) and using Eqs. (70), (31), and Eqs.(16)–(18). Figure 14 shows that the (noiseless) reconstructed profile (dotted curve) coincides with the Stenzel profile (solid curve), and that the recovered profile using the noisy pressure points (dashed-dotted curve) is very similar to the other two curves. The method appears to be robust for noise contamination. Figure 15 shows the corresponding polar plot of the velocity profile of Fig. 14. The solid curve in Fig. 15 is for the near field (r = 0.0975 m) and the dotted curve for the far- field ($r = 1$ m). It appears that the near field is more directive than the far field.

7. EXTENSION TO NON-AXIALLY SYMMETRIC PROFILES

Loudspeaker membranes vibrate mainly in a radially symmetric fashion, in particular at low frequencies. At higher frequencies, break-up behavior can become manifest, and then it may be necessary to consider non-radially symmetric profiles. In the present context, where a loudspeaker is modeled as consisting of a rigid spherical cabinet with a

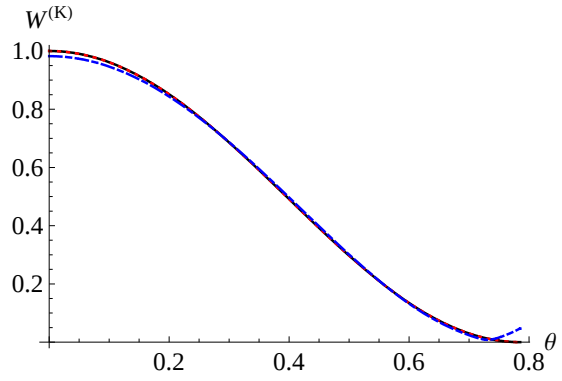

Fig. 14: Stenzel profile $W^{(K)}/(K+1)$ ($K=2$ and $\theta_0=\pi/4$) of Eq. (72) using Eq. (20) directly (solid curve) together with the reconstructed profiles $\hat{W}^{(K)}$ without noise (dotted curve) and with noise added to the pressure points $\hat{p}_j$ (dashed-dotted curve). The (noiseless) reconstructed profile (dotted curve) coincides with the input profile (solid curve).

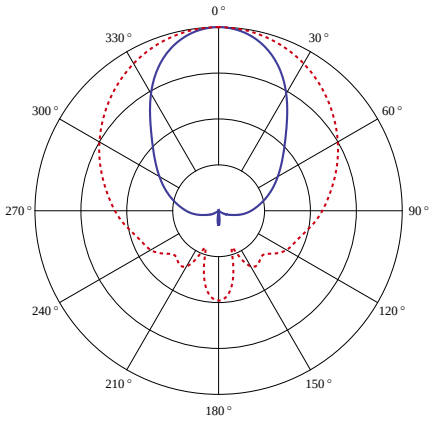

Fig. 15: Polar plots (10 dB/div.) in the near field (solid curve, $r=0.0975$ m) and in the far field (dotted curve, $r=1$ m), corresponding to the parameters of the simulation example and the velocity profile of Fig. 14. All curves are normalized such that the SPL is 0 dB at θ=0.

flexible spherical cap, this requires consideration of non-axially symmetric velocity profiles $V(\theta,\varphi)$ and $W(\theta,\varphi)$ on S_0. This is beyond the scope of the present paper and is discussed elsewhere [20].

8. CONCLUSIONS

Appropriately warped Legendre polynomials provide an efficient and robust method to describe velocity profiles of a flexible spherical cap on a rigid sphere. Only a few coefficients are necessary to approximate various velocity profiles. The polar plot of a rigid spherical cap on a rigid sphere has been shown to be quite similar to that of a real loudspeaker, and is useful in the full 4π-field. The spherical-cap model yields polar plots that exhibit good full range similarity with the polar plots from real loudspeakers. It thus outperforms the more conventional model in which the loudspeaker is modeled as a rigid piston in an infinite baffle. The cap model can be used to predict, besides polar plots, various other acoustical quantities of a loudspeaker. These quantities include the sound pressure, baffle-step response, sound power, directivity, and the acoustic center. At low frequencies ($kR \leq 0.4$) the acoustic center for a loudspeaker lies about 0–0.5 R in front of the loudspeaker, where R is the radius in the case of a spherical cabinet, or some other dimensional measure of the cabinet. At higher frequencies the acoustic center shifts further away from the loudspeaker. The method presented herein enables one to solve the inverse problem of calculating the actual velocity profile of the cap radiator using (measured) on- and off-axis sound pressure data. This computed velocity profile allows the extrapolation to far-field loudspeaker pressure data, including off-axis behavior. Because the pressure data can be collected in the (relative) near-field of a loudspeaker, this avoids the use of anechoic rooms that would be necessary if the far-field were to be assessed directly.

ACKNOWLEDGMENTS

The authors wish to thank Okke Ouweltjes for assisting in the loudspeaker measurements and making the plot for Fig. 1a, and Prof. Fred Simons for providing pertinent assistance in programming Mathematica, in particular to make Fig. 14.

9. REFERENCES

[1] J.W.S. Rayleigh. *The Theory of Sound, Vol. 2,*

1896. (reprinted by Dover, New York), 1945.

[2] L.V. King. On the acoustic radiation field of the piezo-electric oscillator and the effect of viscosity on transmission. *Can. J. Res.*, 11:135–155, 1934.

[3] A. Schoch. Contemplations on the sound field of piston membranes (published in German as Betrachtungen über das Schallfeld einer Kolbenmembran). Akust. Z. 6, 318-326 (1941).

[4] Peter H. Rogers, and A.O. Williams, Jr. Acoustic field of circular plane piston in limits of short wavelength or large radius. *J. Acoust. Soc. Am.*, 52(3B):865–870, 1972.

[5] M. Greenspan. Piston radiator: Some extensions of the theory. *J. Acoust. Soc. Am.*, 65(3):608–621, 1979.

[6] G.R. Harris. Review of transient field theory for a baffled planar piston. *J. Acoust. Soc. Am.*, 70(1):10–20, 1981.

[7] R. New, R.I. Becker, and P. Wilhelmij. A limiting form for the nearfield of the baffled piston. *J. Acoust. Soc. Am.*, 70(5):1518–1526, Nov. 1981.

[8] T. Hasegawa, N. Inoue, and K. Matsuzawa. A new rigorous expansion for the velocity potential of a circular piston source. *J. Acoust. Soc. Am.*, 74(3):1044–1047, September 1983.

[9] D.A. Hutchins, H.D. Mair, P.A. Puhach, and A.J. Osei. Continuous-wave pressure fields of ultrasonic transducers. *J. Acoust. Soc. Am.*, 80(1):1–12, July 1986.

[10] R. C. Wittmann, and A. D. Yaghjian. Spherical-wave expansions of piston-radiator fields. *J. Acoust. Soc. Am.*, 90(3):1647–1655, September 1991.

[11] R.M. Aarts, and A.J.E.M. Janssen. Approximation of the Struve function $\mathbf{H}_1$ occurring in impedance calculations. *J. Acoust. Soc. Am.*, 113(5):2635–2637, May 2003.

[12] T. Hélie, and X. Rodet. Radiation of a pulsating portion of a sphere: Application to horn radiation. *Acta Acustica united with Acustica*, 89(4), 565–577, July/August 2003

[13] R.J. McGough, T.V. Samulski, and J.F. Kelly. An efficient grid sectoring method for calculations of the near-field pressure generated by a circular piston. *J. Acoust. Soc. Am.*, 115(5):1942–1954, May 2004.

[14] T.D. Mast, and F. Yu. Simplified expansions for radiation from a baffled circular piston. *J. Acoust. Soc. Am.*, 118:3457–3464, 2005.

[15] T.J. Mellow. On the sound field of a resilient disk in an infinite baffle. *J. Acoust. Soc. Am.*, 120:90–101, 2006.

[16] J.F. Kelly, and R.J. McGough. An annular superposition integral for axisymmetric radiators. *J. Acoust. Soc. Am.*, 121:759–765, 2007.

[17] Xiaozheng Zeng, and R.J. McGough. Evaluation of the angular spectrum approach for simulations of near-field pressures. *J. Acoust. Soc. Am.*, 123(1):68–76, January 2008.

[18] R.M. Aarts, and A.J.E.M. Janssen. On-axis and far-field sound radiation from resilient flat and dome-shaped radiators. *J. Acoust. Soc. Am.*, 125(3):1444–1455, March 2009.

[19] R.M. Aarts, and A.J.E.M. Janssen. Sound radiation quantities arising from a resilient circular radiator. *J. Acoust. Soc. Am.*, 126(4):1776–1787, Oct. 2009.

[20] R.M. Aarts, and A.J.E.M. Janssen. Sound radiation from a resilient spherical cap on a rigid sphere. *J. Acoust. Soc. Am.*, 127(4), April 2010.

[21] R.M. Aarts, and A.J.E.M. Janssen. Estimating the velocity profile and acoustical quantities of a harmonically vibrating loudspeaker membrane from on-axis pressure data. *J. Audio Eng. Soc.*, 57(12):1004–1015, December 2009.

[22] P.M. Morse, and H. Feshbach. *Methods of theoretical physics*. McGraw-Hill, 1953.

[23] H. Stenzel, and O. Brosze. *Guide to computation of sound phenomena (published in German as Leitfaden zur Berechnung von Schallvorgängen), 2nd ed.* Springer-Verlag, Berlin, 1958.

[24] P.M. Morse, and K.U. Ingard. *Theoretical acoustics*. McGraw-Hill Book Company, New York, 1968.

[25] E. Skudrzyk. *The Foundations of Acoustics*. Springer-Verlag, New York, 1971, ASA-reprint 2008.

[26] L.E. Kinsler, A.R. Frey, A.B. Coppens, and J.V. Sanders. *Fundamentals of Acoustics*. Wiley, New York, 1982.

[27] A.D. Pierce. *Acoustics, An Introduction to Its Physical Principles and Applications*. Acoustical Society of America through the American Institue of Physics, 1989.

[28] D.T. Blackstock. *Fundamentals of physical Acoustics*. John Wiley & Sons, New York, 2000.

[29] F.J.M. Frankort. *Vibration and Sound Radiation of Loudspeaker Cones*. Ph.D. dissertation, Delft University of Technology, 1975.

[30] M. Abramowitz, and I.A. Stegun. *Handbook of Mathematical Functions*. Dover, New York, 1972.

[31] Harry F. Olson. Direct radiator loudspeaker enclosures. *J. Audio Eng. Soc.* 17(1), 22–29, Jan. 1969.

[32] A.J.E.M. Janssen, and P. Dirksen. Concise formula for the Zernike coefficients of scaled pupils. *J. Microlith., Microfab., Microsyst.*, 5(3), 030501, July-Sept. 2006.

[33] A.J.E.M. Janssen, S. van Haver, P. Dirksen, and J.J.M. Braat. Zernike representation and Strehl ratio of optical systems with variable numerical aperture. *J. of Modern Optics*, 55(7), 1127–1157, April 2008.

[34] Finn Jacobsen, Salvador Barrera Figueroa, and Knud Rasmussen. A note on the concept of acoustic center. *J. Acoust. Soc. Am.*, 115(4):1468–1473, April 2004.

[35] John Vanderkooy. The acoustic center: A new concept for loudspeakers at low frequencies. *AES* Convention paper 6912 presented at the 121$^{\text{th}}$ Convention, San Francisco, Oct. 5–8, 2006.